Journal of Membrane Science 603 (2020) 118011

Contents lists available at ScienceDirect

Journal of Membrane Science

journal homepage: http://www.elsevier.com/locate/memsci

The synergistic effect of protonated imidazole-hydroxyl-quaternary ammonium on improving performances of anion exchange membrane assembled flow batteries

Yue Du [a,b], Li Gao [a], Lei Hu [a], Mengting Di [a], Xiaoming Yan [a,c,**], Baigang An [b,***], Gaohong He [a,c,*]

[a] State Key Laboratory of Fine Chemicals, School of Chemical Engineering, Dalian University of Technology, 2 Dagong Road, Panjin, LN, 124221, China
[b] School of Chemical Engineering, University of Science and Technology Liaoning, 185 Qianshangzhong Road, Anshan, 114051, China
[c] Panjin Institute of Industrial Technology, Dalian University of Technology, 2 Dagong Road, Panjin, LN, 124221, China

ARTICLE INFO

Keywords:
Polybenzimidazole
Vanadium redox flow battery
Synergistic effect
Anion exchange membranes

ABSTRACT

Protonated imidazole-hydroxyl-quaternary ammonium co-functionalized polybenzimidazole (PBI) anion exchange membranes are designed for vanadium redox flow battery (VFB). The structure is achieved by grafting glycidyl trimethyl ammonium chloride onto the PBI on basic of open-ring reaction. The synergistic effect of the protonated imidazole-hydroxyl-quaternary ammonium is supposed to create proton transport channels with hydrogen bonding and Donnan exclusion effect, leading to high proton conductivity and low vanadium permeability of the membrane. The single cell employing this membrane reveals a high performance with a coulombic efficiency of 99.3% and an energy efficiency of more than 80% at 200 mA cm^{-2}. A long-term life of over 500 cycles at 120 mA cm^{-2} could be attributed to the good chemical stability of the membrane. These results indicate the membrane proposed here is a promising choice for VFB application.

1. Introduction

The energy storage devices are needed for stable output of turbulent alternative solar and wind energies [1]. Redox flow battery (RFB) attracts attention for the long life, high efficiency and safety [2–5]. Compared to other metal ion pairs, vanadium ions of different valence states are used as electrolytes, avoiding cross-contamination between electrolytes in anode and cathode for vanadium flow battery (VFB) [2,6–10]. The membrane is a core component of the battery. It not only separates vanadium ion of the bipolar electrolytes, but also allows proton to shuttle back and forth between anode and cathode [11,12]. The ideal ion exchange membrane should possess low vanadium permeability, low cost, high proton conductivity, excellent mechanical property and chemical stability [13–18]. Perfluorosulfonic acid membranes represented by Nafion from DuPont have been widely used in VFB as a result of outstanding chemical stability and high proton conductivity [19–21]. However, severe vanadium permeation leads to imbalance of electrolytes and battery capacity fading as well as low columbic efficiency. Besides, the high price of perfluorosulfonic acid membrane also hinders the applications in VFB [21–23]. There have been a variety of the strategies that have been explored to prepare alternative membrane materials, such as polyvinylidene fluoride (PVDF) [24–26], polytetrafluoroethylene (PTFE) [27], polysufone (PSF) [28] and poly (ether ether ketone) (PEEK) [29]. The proton-selective and cost-effective membrane is urgently needed for large-scale application of VFB [30,31].

To solve the issues of vanadium permeation and cost, positively charged functional groups (such as quaternary ammonium) are introduced into nonperfluorinated polymers backbone [32–34]. It can repel the vanadium ion under the effect of Donnan exclusion to improve the columbic efficiency (CE) of VFB [30,35,36]. Zhang et al. prepared an aromatic polymer-based quaternized anion exchange membranes,

* Corresponding author. State Key Laboratory of Fine Chemicals, School of Chemical Engineering, Dalian University of Technology, 2 Dagong Road, Panjin, LN, 124221, China.
** Corresponding author. State Key Laboratory of Fine Chemicals, School of Chemical Engineering, Dalian University of Technology, 2 Dagong Road, Panjin, LN, 124221, China.
*** Corresponding author.
E-mail addresses: yanxiaoming@dlut.edu.cn (X. Yan), bgan@ustl.edu.cn (B. An), hgaohong@dlut.edu.cn (G. He).

https://doi.org/10.1016/j.memsci.2020.118011
Received 9 December 2019; Received in revised form 13 February 2020; Accepted 29 February 2020
Available online 5 March 2020

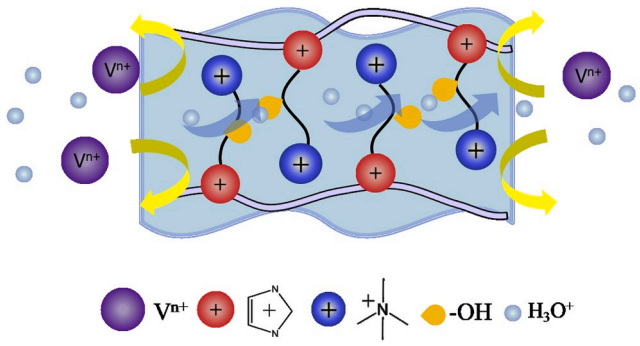

Scheme 1. Diagram of bi-functionalized membrane containing abundant hydroxyl and quaternary ammonium groups.

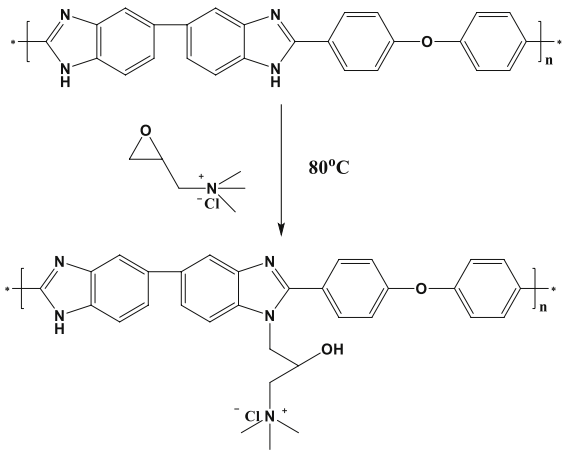

Scheme 2. Synthesis of PBI-GTA-x.

which displayed a voltage efficiency (VE) up to 81.9% and a CE up to 98.3% at 140 mA cm^{-2} [37]. Li et al. fabricated AEMs having PTA groups in the side chain (PSf-c-PTA) and the prepared AEMs showed a considerable batteries efficiency with a CE of >98% and VE of 85.6% at 120 mA cm^{-2} [38]. Lee et al. successfully prepared an ether-free poly (*p*-phenylene)-based anion exchange membrane, which achieved a CE even near to 100% and a VE up to 87% at 80 mA cm^{-2} [39]. The protonated amine groups with positively charge could also repulse vanadium ions. Zhao et al. used protonated polybenzimidazole (PBI) membranes in VFB, obtaining a CE reached 99% and a VE up to 79% at 40 mA cm^{-2} [40]. However, for high current density operation in VFB application, there is still a need to further improve VE of membranes [41].

Very recently, hydroxyl groups have been confirmed to form hydrogen bond networks in the hydrophilic channels to promote proton transport [26]. Inspired by the Donnan effect of positively charged groups and hydrogen bond donor ability of hydroxyl groups, a novel membrane with protonated imidazole-hydroxyl-quaternary ammonium side chain was herein designed and prepared by grafting glycidyl trimethyl ammonium chloride (GTA) onto the backbone of PBI based on ring-opening reactions. The protonated imidazole-hydroxyl-quaternary ammonium side chain in membrane has a synergistic effect on creating hydrogen bond based proton transport channels as well as Donnan exclusion based vanadium ion barriers (Scheme 1). The nanostructure and morphology of the prepared membrane were investigated in detail. Furthermore, the flow battery performances were assessed by a series of tests. This membrane has a great potential as high-performance material for application of VFB.

Table 1
Reaction conditions and DS of PBI-GTA-x.

Membranes	Mole ratio of the GTA: PBI repeat unit	DS based on[1] H NMR (%)	Reaction time (h)
PBI-GTA-112%	1.5 : 1	112	24
PBI-GTA-93%	1 : 1	93	24
PBI-GTA-67%	1 : 2	67	24
PBI	–	0	0

2. Experimental

2.1. Materials

Polybenzimidazole (PBI) has a molecular weight of 14000 g mol^{-1}, which is supplied by Shanghai Shengjun Plastics Technology Co., Ltd. Glycidyl trimethyl ammonium chloride (GTA) is purchased from Saen Chemical Technology (Shanghai) Co., Ltd. Dimethylsulfoxide (DMSO) is bought from Tianjin Fuyu Fine Chemical Co., Ltd. Acetone is provided by Tianjin Komi Chemical Reagent Co., Ltd.

2.2. Preparation of PBI-GTA-x membranes

GTA was grafted onto the PBI by the following procedure (Scheme 2). 50 mL DMSO was poured into a 100 ml single-necked flask and then 1 g PBI was added into form a 2% solution at 80 °C. After completely dissolved, 0.625 g GTA was added into the flask and continually stirred for 24 h. After the reaction, the resulted solution was precipitated in acetone. The precipitated PBI-GTA-x (where x was the degree of substitution) was washed with deionized water before dried in an oven at 60 °C. A series of PBI-GTA-x were obtained by controlling the amount of GTA (Table 1). Then, 0.11 g PBI-GTA-x polymer was dissolved in 5 mL DMSO and casted in a glass plate. The final obtained membrane was dried in an oven at 60 °C for 48 h before removed from the glass plate. The obtained dry membranes had an average thickness of 30 μm.

2.3. Microstructure and morphology characterization

The ^{1}H NMR spectrum of the polymer dissolved in DMSO-d_6 was tested using a spectrometer (Bruker AVANCE III HD 500). The microstructure of the PBI-GTA-x membranes was tested by JEOL JEM-2000EX microscope. The membranes were immersed in 1 M KI, and dried after washed with deionized water.

2.4. Property measurements

The ion exchange capacity (IEC) of membranes was measured by the titration method. Water uptake (WU) and swelling ratio (SR) were tested in 3 M H_2SO_4 conditions. The area resistance (AR) of membranes with an effective area of 1.766 cm^2 were detected in 3 M H_2SO_4 and calculated as follow: $AR = (R_1 - R_2) \times S$. where R_1 and R_2 is resistances with and without a membrane, respectively. The vanadium permeability of the membrane was evaluated based on our previous work [42].

2.5. Battery test

The battery consisted of 3 × 3 cm^2 membrane, graphite felts and graphite felt electrodes was detected with LANHE CT2001A system. DuPont's Nafion 212 was pretreated as same as the literature [20,43,44]. Positive and negative electrolytes used 50 mL of 1.5 M VO_2^+/VO^{2+} in 3 M H_2SO_4 solution and equivalent amount of 1.5 M V^{3+}/V^{2+} in 3 M H_2SO_4 solution, respectively. The current density range is 40–200 mA cm^{-2} and the cut-off voltage is 1.00–1.55 V for flow battery. The cycle is tested at 120 mA cm^{-2}. The self-discharge test was measured at 50%

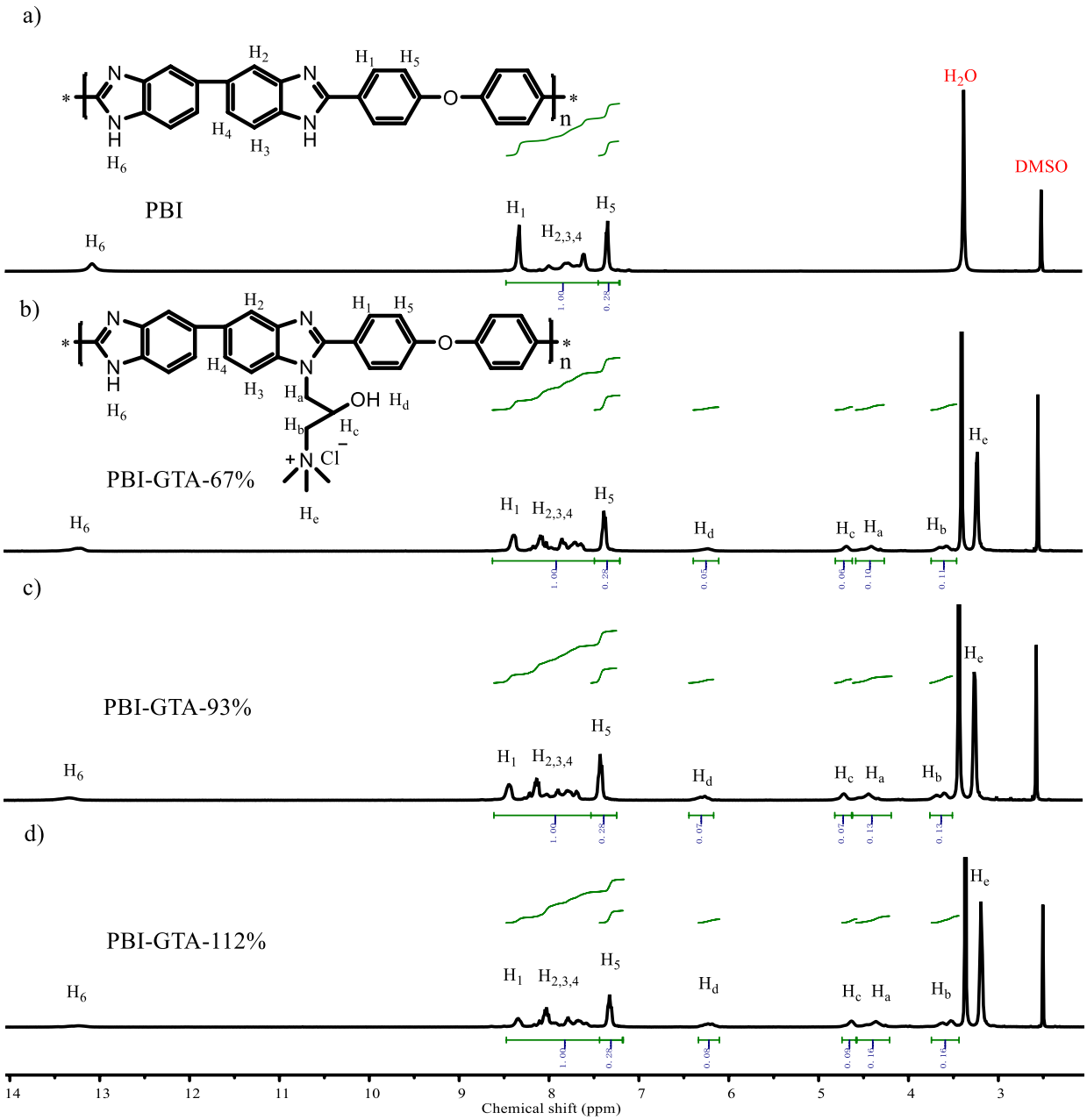

Fig. 1. ^{1}H NMR spectra of a) PBI, b) PBI-GTA-67%, c) PBI-GTA-93% and d) PBI-GTA-112% membranes.

state of charge (SOC) until dropping to 0.8 V.

2.6. Chemical stability

Chemical stability was tested by immersing the membranes in 1.5 M VO_2^+/3 M H_2SO_4 solutions. After 32 days, the membrane was washed with deionized water and then dried at 60 °C. The weight of membranes (W_0 and W before and after immersion) was recorded, and weight change was calculated as follow:

$$Weight\ change = \frac{W - W_0}{W_0} \times 100\%$$

3. Results and discussion

3.1. Structural confirmation

Fig. 1 shows the ^{1}H NMR spectra of PBI and PBI-GTA-x. The characteristic signal attributed to N–H proton on the PBI backbone was at 13.23 ppm (Fig. 1a) and significantly weakened after the grafting reaction (Fig. 1b–d). New characteristic peaks at 6.24 ppm (H_d), 4.63 ppm (H_c), 4.36 ppm (H_a), 3.6 ppm (H_b) and 3.18 ppm (H_e) correspond to methyl protons, methylene protons and hydroxyl groups of the side chain. These confirmed the successful ring-opening reactions of GTA onto the backbone of PBI. It is worth noting that the characteristic peaks from 7.58 ppm to 8.33 ppm (H_1–H_4) in Fig. 1b–d shows a significant change compared with Fig. 1a, which was caused by the interaction between the main chain and the side chains. However, the characteristic peak at 7.3 ppm (H_5) remained unchanged after grafting indicates that H_5 is rarely affected by side chain. The degree of substitution (DS) was calculated to be 112%, 93%, and 67% as: $DS = 2S(H_a)/S(H_5)$, where S (H_a) and $S(H_5)$ represent the integral areas of H_a and H_5 peaks, respectively.

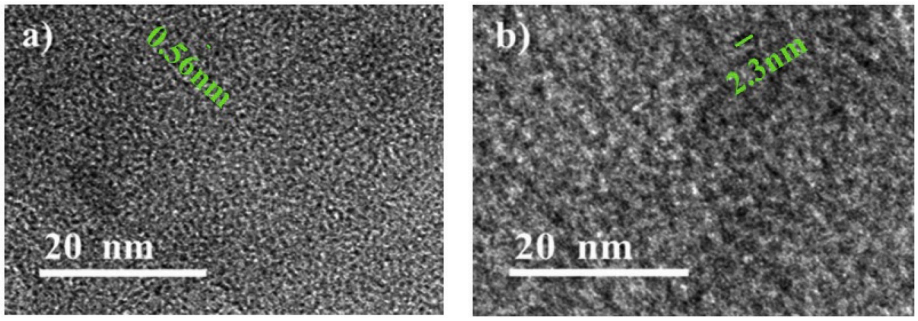

Fig. 2. TEM images of (a) PBI-GTA-67% and (b) PBI-GTA-112% membranes.

Table 2
IEC, SR, WU and Conductivity of PBI-GTA-x and PBI membranes.

Membrane	IEC_t[a] (mmol g^{-1})	IEC_e[b] (mmol g^{-1})	SR (%)	WU (%)	Conductivity[c] (mS cm^{-1})
PBI-GTA-112%	2.82	2.40	19	30	9.68
PBI-GTA-93%	2.39	2.10	15	26	7.90
PBI-GTA-67%	1.90	1.86	13	24	5.46
PBI	–	–	7	18	3.00

[a] Theoretical IEC (IEC_t) are calculated from ^{1}H NMR.
[b] Experimental IEC (IEC_e) are measured by back-titration method at room temperature.
[c] Conductivity is calculated as: $\sigma = L/(R \cdot S)$, where L, R, S are the thickness, resistance and cross-sectional area of the membrane, respectively).

3.2. Morphology of PBI-GTA-x membrane

The membranes morphologies were analyzed by TEM (Fig. 2). The hydrophilic domains of the anion and hydroxyl groups contribute to dark regions, while the hydrophobic backbone is attributed to bright regions. It could be observed that the ion clusters disperse within the hydrophobic domains, forming a nanophase separation structure. The size of the hydrophilicity phase of membrane was roughly measured to be ~2 nm for PBI-GTA-112% and ~0.6 nm for PBI-GTA-67%. As described in our previous work [42], pristine PBI membrane had no obvious nanophase separation structure, suggesting that the introduction GTA side chain improved the nanophase separation structure. As the degree of substitution increased, the ion cluster became larger and more continuous, which constructed a better nanophase separation structure to facilitate proton transport.

3.3. Membrane properties

The basic performance of the membranes is listed in Table 2. The IEC mainly depends on the number of cationic groups in membrane and has a large extent effect on the ion conductivity and WU of membrane. Water is required in the membrane to form an ion transport channel. The IEC increases with increasing the DS of membranes. The increased WU was conducive to the construction of ion channels in the membrane to promote ion transport. As the increasing of DS, the WU of membrane increased from 18% of PBI to 30% of PBI-GTA-112%. However, an excessive WU might cause a high SR, reducing the mechanical properties of the membrane. The SR of membrane increased from 7.4% for PBI to 19% for PBI-GTA-112%. This should be associated with the introduction of the side chains which have abundant hydroxyl groups and quaternary ammonium groups. The imidazole-hydroxyl-quaternary ammonium could form strong hydrogen bond with water molecules, resulting high SR and WU. Originating for the enhanced WU, the conductivity of PBI-GTA-112% membrane is more than three times higher than that of the PBI-based membrane. It suggested that the good ion transport channels and hydrogen bond promoting effect of hydroxyl groups obviously

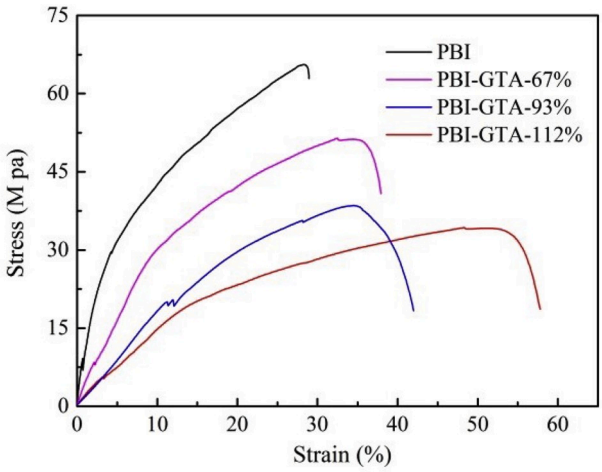

Fig. 3. Stress-strain curves of PBI and PBI-GTA-x membranes.

Table 3
Mechanical properties of PBI and PBI-GTA-x membrane.

Membrane	Tensile strength (M Pa)	Elongation (%)	Elastic modulus (M Pa)
PBI-GTA-112%	34	58	136
PBI-GTA-93%	38	42	183
PBI-GTA-67%	51	39	275
PBI	65	29	685

enhanced the proton conductivity in the membrane. For the long-term stability in VFB operations, the mechanical properties of membranes were presented in Fig. 3 and Table 3. The tensile strength of pure PBI we measured was a little low, but still within the normal range [45–47]. The tensile strength and elastic modulus of all the PBI-GTA membranes were high enough for maintaining the reasonable toughness for VFB application, although they partially decreased. The elongation at break increased significantly from 29% to 58%, improving the impact resistance of the membranes.

The area resistance (AR) of the PBI-GTA-x and PBI membranes was shown in Fig. 4a. As the DS increased, the AR of the PBI-GTA-x membranes obviously decreased from 0.9 Ω cm^2 of PBI to 0.31 Ω cm^2 of PBI-GTA-112%. Such a low area resistance is comparable to that of Nafion 212 (0.22 Ω cm^2). The vanadium ion permeability directly affects the CE and self-discharge rates of the VFB. The permeation of vanadium ion was measured across membrane and the relationship between the concentration and the function of time were obtained (Fig. 4b). Although the vanadium ion permeability of the PBI-GTA-x membranes slightly increased with the increment of quaternary ammonium and hydroxyl groups, it was still at a very low level. PBI-GTA-112% membrane showed

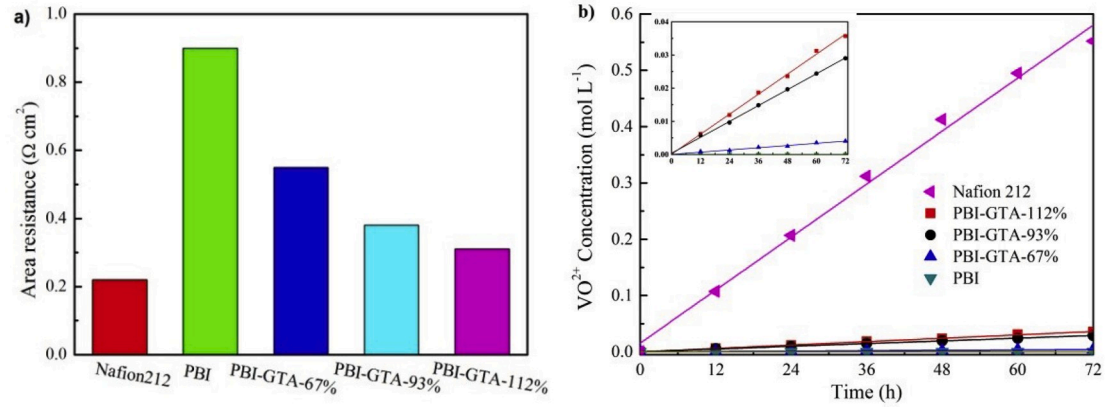

Fig. 4. a) AR and b) VO^{2+} ion diffusion of Nafion 212 and PBI-GTA-x membranes.

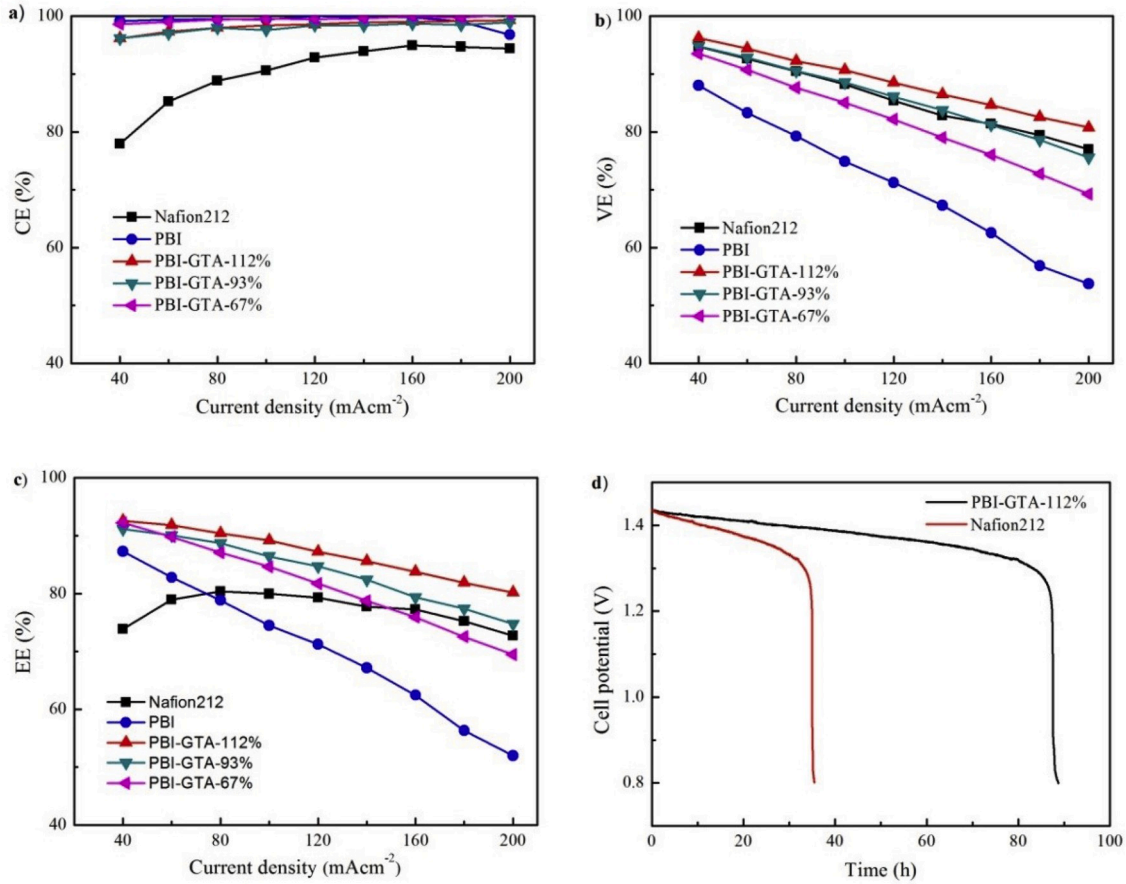

Fig. 5. a) CE, b) VE and c) EE of single-cell performance with PBI-GTA-x and Nafion212 membranes at different current densities; d) OCV of PBI-GTA-112% and Nafion212 membrane.

a permeability of 3.93×10^{-9} cm^2 s^{-1}, which was one order of magnitude lower than that of Nafion 212 (7.76×10^{-8} cm^2 s^{-1}). This is due to the blocking effect of the positively charged protonated imidazole-hydroxyl-quaternary ammonium side chains on vanadium ions. Consequently, enhanced proton conductivity and decreased permeability made the PBI-GTA-x membranes achieve much higher ion selectivity than commercial Nafion 212, resulting high performance in VFB application.

3.4. Single cell performances

The electrochemical performance of the PBI-GTA-x membranes were evaluated at the current density range of 40–200 mA cm^{-2} and compared with that of Nafion 212 (Fig. 5). Compared to Nafion 212, the PBI-GTA-x membranes exhibited higher CE values due to the much lower diffusion coefficient of vanadium ions (Fig. 5a). Even with a high DS, the PBI-GTA-112% membrane displayed higher CE (96.2%–99.3%) than that of Nafion 212 (78.0–94.4%) during the all current densities range. Since Nafion 212 has lower vanadium permeability than at high current density, CE increases significantly at high densities [21,48]. The

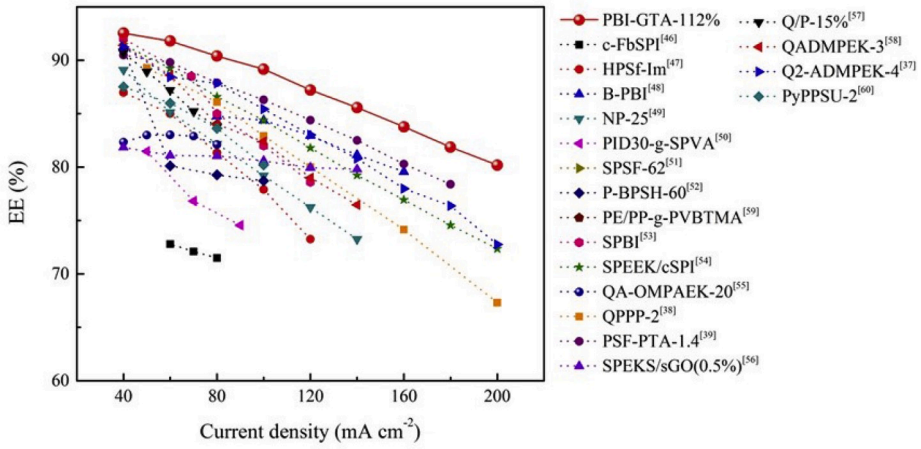

Fig. 6. The comparison of battery performances with anion exchange membranes reported in recent years [37–39,49–63].

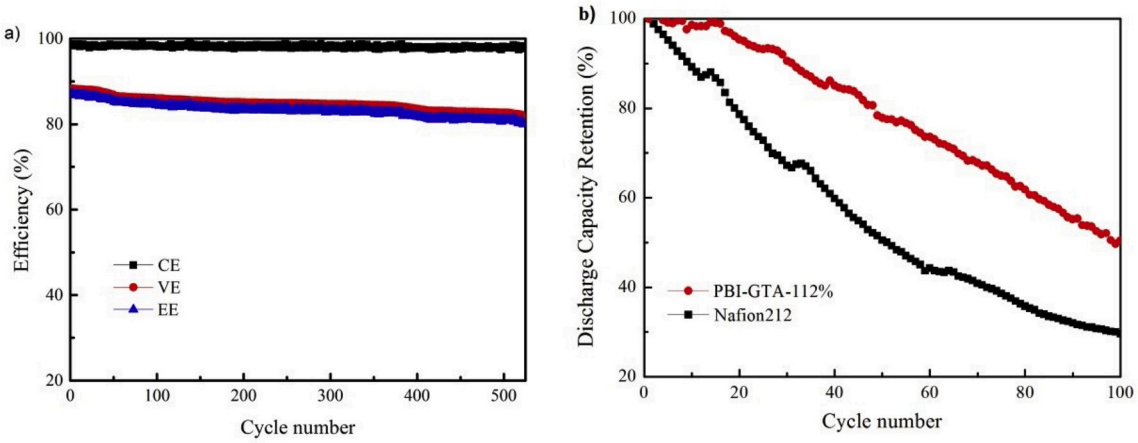

Fig. 7. a) Cycling performance at 120 mA cm^{-2} of the PBI-GTA-112% membrane; b) capacity decay of PBI-GTA-112% and Nafion212 membrane.

CE at low current density is very low. In contrast, there was a slight change of CE for PBI-GTA-x membranes with increasing current density due to the hydrogen bond network and Donnan effect of positively charged side chains. The VE values of the membranes correspond to the IEC values and ionic conductivities of the membranes. As the DS increased, the wider and more connected ion transport channels in the membranes lead to an increase of VE (Fig. 5b). The VE of PBI-GTA-112% membrane decreased from 96.2% to 80.7% at 40–200 mA cm^{-2}, which was caused by larger ohmic polarization at higher current density. The EE is an important evaluation parameter of battery performance and determined by CE and VE. The battery assembled with PBI-GTA-112% membrane exhibited a high EE more than 80% at 200 mA cm^{-2}, which was superior to that of Nafion 212 (Fig. 5c). The self-discharge tests of PBI-GTA-112% and Nafion 212 membranes were also investigated (Fig. 5d). The self-discharge duration time with PBI-GTA-112% membrane was 88 h, which was 150% longer than that of Nafion 212 (35 h), in good agreement with the vanadium ion permeability values. A comprehensive comparison of EE between PBI-GTA-112% and ion exchange membranes reported in recent years was also made (Fig. 6). The cell assembled with PBI-GTA-112% membrane exhibited impressive EE, which showed greater advantages at higher current density. Specifically, the EE of PBI-GTA-112% membrane was still higher than 80% at 200 mA cm^{-2}, while of other membranes had fallen below 80%. The synergistic effect of protonated imidazole-hydroxyl-quaternary ammonium of PBI-GTA-112% membrane leads to high proton conductivity and low vanadium permeability, resulting in satisfactory EE. The excellent performances suggest that PBI-GTA-x membrane with protonated imidazole-hydroxyl-quaternary ammonium side chain is promising for use in practical VFB system.

3.5. Cycle performance

The cycling performance of the PBI-GTA-112% membrane was tested at 120 mA cm^{-2} (Fig. 7). The cell assembled with PBI-GTA-112% membrane displayed a stable CE of >98% over 500 cycles (Fig. 7a). Capacity decay is another key indicator for evaluating flow battery performance (Fig. 7b). Although a gradual capacity fade was caused by the vanadium across the membrane, the capacity retention of the PBI-GTA-112% membrane was much higher compared to the Nafion 212 membrane. The capacity retention assembled with PBI-GTA-112% membrane was 78% after 50 cycles, which was nearly 30% higher than that of Nafion 212 (50%).

3.6. Chemical stability

The PBI-GTA-x membranes were immersed in 1.5 M VO_2^+/3 M H_2SO_4 solution for 32 days at room temperature to test their chemical stability (Fig. 8). The membranes become darker due to the absorption of vanadium ions (Fig. 8a and b). The morphology of the membrane still remained robust. The mass change of membranes was measured and the corresponding values were all below 10% (Fig. 8c). The FTIR spectra of PBI, PBI-GTA-112% and PBI-GTA-112% membranes after 500 cycles

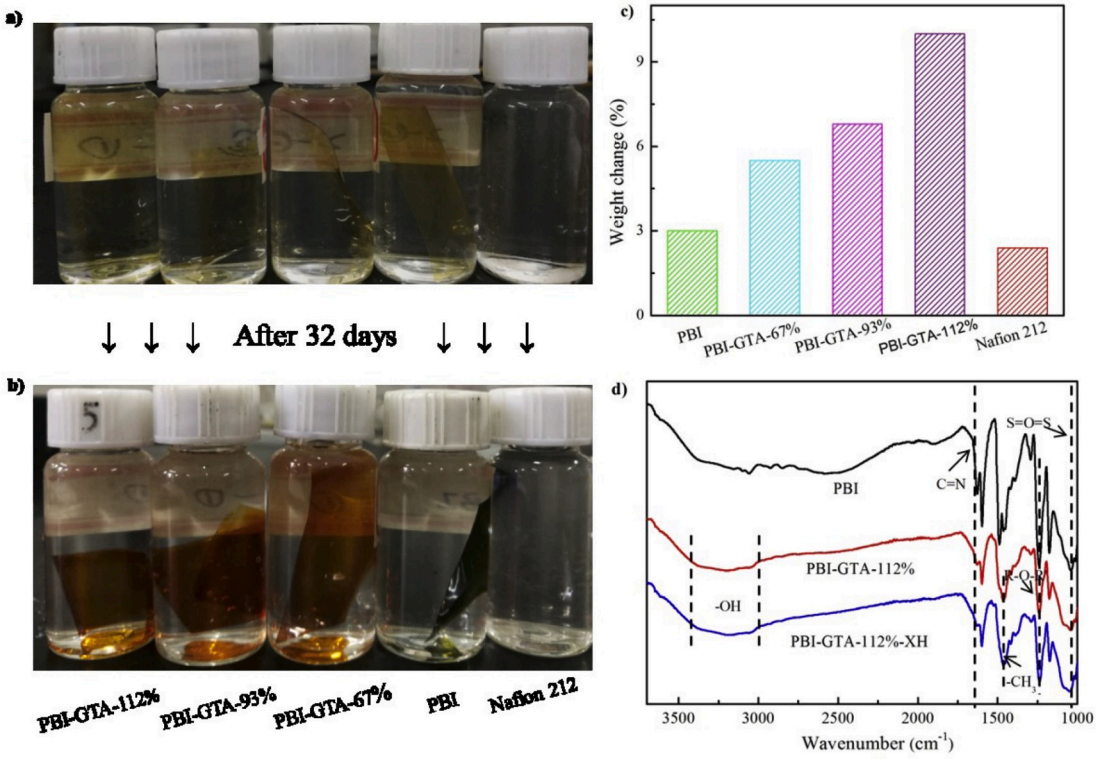

Fig. 8. PBI-GTA-x and Nafion 212 membranes: a) before and b) after immersing in 1.5 M VO_2^+/3 M H_2SO_4 solution after 32 days; c) the corresponding weight change of PBI-GTA-x and Nafion 212; d) FTIR spectra of PBI, PBI-GTA-112% and PBI-GTA-112% after 500 cycles.

were detected to further investigate the operational stability of the membrane (Fig. 8d). The stretching vibration of the C═N and ether linkage reflected the characteristic absorptions at 1630 cm^{-1} and 1167 cm^{-1}, respectively. The characteristic absorptions at 1460 cm^{-1} and 3300 cm^{-1} were attributed to –CH_3 and –OH of side chain in PBI-GTA-112% membranes, respectively [47]. Due to the sulfuric acid treatment, the vibration of S═O═S appeared at 1036 cm^{-1} [64]. There was no obvious change in the FTIR spectra for the PBI-GTA-112% membrane after 500 cycles compared to the pristine PBI-GTA-112% membrane. These indicated this membranes exhibits good chemical stability under strong acid and strong oxidation conditions.

4. Conclusion

A novel anion exchange membrane containing protonated imidazole-hydroxyl-quaternary ammonium side chain was designed to improve proton conductivity and hinder vanadium ions for VFB. The glycidyl trimethyl ammonium chloride was grafted onto the PBI, which promoted the formation of hydrophilic/hydrophobic phase-separation structure. The protonated imidazole-hydroxyl-quaternary ammonium side chain could facilitate proton transport and VO^{2+} exclusion by hydrogen netwok and Donnan effect. Thereby, the membrane prepared here obtained low vanadium penetration (3.93×10^{-9} cm^2 s^{-1}) and area resistance (0.31 Ω cm^2), which led to excellent efficiency. The cell assembled with PBI-GTA-112% membrane exhibited an excellent a EE higher than 80% at 200 mA cm^{-2} and displayed a stable CE (>98%) over 500 cycles at 120 mA cm^{-2}. It indicates that this membrane has a great application prospect in flow battery.

Declaration of competing interest

The authors declare that they have no known competing financial interests or personal relationships that could have appeared to influence the work reported in this paper.

CRediT authorship contribution statement

Yue Du: Conceptualization, Validation, Writing - original draft, Formal analysis. **Li Gao:** Validation, Investigation, Formal analysis. **Lei Hu:** Writing - original draft, Investigation, Formal analysis. **Mengting Di:** Investigation, Formal analysis. **Xiaoming Yan:** Writing - review & editing, Funding acquisition, Project administration. **Baigang An:** Writing - review & editing. **Gaohong He:** Writing - review & editing, Funding acquisition.

Acknowledgements

This work was supported by the National Natural Science Foundation of China (grant no. U1808209, U1663223, 21527812, and 21706023), National Key Research and Development Program of China (grant no. 2016YFB0101203) and Fundamental Research Funds for the Central Universities (grant no. DUT18JC40).

References

[1] C. Liu, F. Li, L.P. Ma, H.M. Cheng, Advanced materials for energy storage, Adv. Mater. 22 (2010) E28–E62.
[2] V. Aravindan, J. Gnanaraj, Y.-S. Lee, S. Madhavi, $LiMnPO_4$ – a next generation cathode material for lithium-ion batteries, J. Mater. Chem. 1 (2013) 3518–3539.
[3] Y. Ding, C. Zhang, L. Zhang, Y. Zhou, G. Yu, Molecular engineering of organic electroactive materials for redox flow batteries, Chem. Soc. Rev. 47 (2018) 69–103.
[4] C. Zhang, L. Zhang, Y. Ding, S. Peng, X. Guo, Y. Zhao, G. He, G. Yu, Progress and prospects of next-generation redox flow batteries, Energy Storage Mater. 15 (2018) 324–350.
[5] Y. Ding, C. Zhang, L. Zhang, Y. Zhou, G. Yu, Pathways to widespread applications: development of redox flow batteries based on new chemistries, Inside Chem. 5 (2019) 1964–1987.
[6] K. Gong, Q. Fang, S. Gu, S.F.Y. Li, Y. Yan, Nonaqueous redox-flow batteries: organic solvents, supporting electrolytes, and redox pairs, Energy Environ. Sci. 8 (2015) 3515–3530.
[7] M. Park, J. Ryu, W. Wang, J. Cho, Material design and engineering of next-generation flow-battery technologies, Nat. Rev. Mater. 2 (2016) 1680–1697.
[8] W. Wang, Q. Luo, B. Li, X. Wei, L. Li, Z. Yang, Recent progress in redox flow battery Research and development, Adv. Funct. Mater. 23 (2013) 970–986.

[9] L. Zhang, Y. Ding, C. Zhang, Y. Zhou, X. Zhou, Z. Liu, G. Yu, Enabling graphene-oxide-based membranes for large-scale energy storage by controlling hydrophilic microstructures, Inside Chem. 4 (2018) 1035–1046.

[10] L. Zhang, C. Zhang, Y. Ding, K. Ramirez-Meyers, G. Yu, A low-cost and high-energy hybrid iron-aluminum liquid battery achieved by deep eutectic solvents, Joule 1 (2017) 623–633.

[11] I.S. Chae, T. Luo, G.H. Moon, W. Ogieglo, Y.S. Kang, M. Wessling, Ultra-high proton/vanadium selectivity for hydrophobic polymer membranes with intrinsic nanopores for redox flow battery, Adv. Energy Mater. 6 (2016) 1600517–1600522.

[12] X.L. Zhou, T.S. Zhao, L. An, Y.K. Zeng, L. Wei, Critical transport issues for improving the performance of aqueous redox flow batteries, J. Power Sources 339 (2017) 1–12.

[13] S. Gu, B. Xu, Y. Yan, Electrochemical energy engineering: a new frontier of chemical engineering innovation, Annu. Rev. Chem. Biomol. Eng. 5 (2014) 429–454.

[14] X. Li, H. Zhang, Z. Mai, H. Zhang, I. Vankelecom, Ion exchange membranes for vanadium redox flow battery (VRB) applications, Energy Environ. Sci. 4 (2011) 1147–1160.

[15] A. Tang, J. Bao, M. Skyllas-Kazacos, Studies on pressure losses and flow rate optimization in vanadium redox flow battery, J. Power Sources 248 (2014) 154–162.

[16] T. Mohammadi, S.C. Chieng, M. Skyllas-Kazacos, Water transport study across commercial ion exchange membranes in the vanadium redox flow battery, J. Membr. Sci. 133 (1997) 151–159.

[17] T. Mohammadi, M. Skyllas-Kazacos, Evaluation of the chemical stability of some membranes in vanadium solution, J. Appl. Electrochem. 27 (1997) 153–160.

[18] T. Mohammadi, M. Skyllas-Kazacos, Modification of anion-exchange membranes for vanadium redox flow battery applications, J. Power Sources 63 (1996) 179–186.

[19] Q. Luo, L. Li, W. Wang, Z. Nie, X. Wei, B. Li, B. Chen, Z. Yang, V. Sprenkle, Capacity decay and remediation of nafion-based all-vanadium redox flow batteries, ChemSusChem 6 (2013) 268–274.

[20] B. Jiang, L. Yu, L. Wu, D. Mu, L. Liu, J. Xi, X. Qiu, Insights into the impact of the nafion membrane pretreatment process on vanadium flow battery performance, ACS Appl. Mater. Interfaces 8 (2016) 12228–12238.

[21] B. Jiang, L. Wu, L. Yu, X. Qiu, J. Xi, A comparative study of Nafion series membranes for vanadium redox flow batteries, J. Membr. Sci. 510 (2016) 18–26.

[22] N.N. Intan, K. Klyukin, T.J. Zimudzi, M.A. Hickner, V. Alexandrov, A combined theoretical-experimental study of interactions between vanadium ions and Nafion membrane in all-vanadium redox flow batteries, J. Power Sources 373 (2018) 150–160.

[23] K.A. Mauritz, R.B. Moore, State of understanding of nafion, Chem. Rev. 104 (2004) 4535–4586.

[24] F. Long, Y. Fan, B. Wang, PVDF based ion exchange membrane for all vanadium redox flow battery, Battery Bimon 39 (2009) 68–70.

[25] Y. Lai, L. Wan, B. Wang, PVDF/Graphene composite nanoporous membranes for vanadium flow batteries, Membranes 9 (2019) 1–13.

[26] S. Li, L. Chu, X. Gong, D. Ulrike, Hydrogen bonding controls the dynamics of catechol adsorbed on a TiO_2 (110) surface, Science 328 (2010) 882–884.

[27] J. Qiu, L. Zhao, M. Zhai, J. Ni, H. Zhou, J. Peng, J. Li, G. Wei, Pre-irradiation grafting of styrene and maleic anhydride onto PVDF membrane and subsequent sulfonation for application in vanadium redox batteries, J. Power Sources 177 (2008) 617–623.

[28] S.W. Choi, T.H. Kim, S.W. Jo, J.Y. Lee, S.H. Cha, Y.T. Hong, Hydrocarbon membranes with high selectivity and enhanced stability for vanadium redox flow battery applications: comparative study with sulfonated poly(ether sulfone)s and sulfonated poly(thioether ether sulfone)s, Electrochim. Acta 259 (2018) 427–439.

[29] Z.Z. Yuan, X.F. Li, J.B. Hu, W.X. Xu, J.Y. Cao, H.M. Zhang, Degradation mechanism of sulfonated poly(ether ether ketone) (SPEEK) ion exchange membranes under vanadium flow battery medium, Phys. Chem. Chem. Phys. 16 (2014) 19841–19847.

[30] D. Chen, M.A. Hickner, E. Agar, E.C. Kumbur, Selective anion exchange membranes for high coulombic efficiency vanadium redox flow batteries, Electrochem. Commun. 26 (2013) 37–40.

[31] D. Chen, S. Kim, L. Li, G. Yang, M.A. Hickner, Stable fluorinated sulfonated poly (arylene ether) membranes for vanadium redox flow batteries, RSC Adv. 2 (2012) 8087–8094.

[32] N. Li, M.D. Guiver, Ion transport by nanochannels in ion-containing aromatic copolymers, Macromolecules 47 (2014) 2175–2198.

[33] X. Yan, C. Zhang, Z. Dong, B. Jiang, Y. Dai, X. Wu, G. He, Amphiprotic side-chain functionalization constructing highly proton/vanadium-selective transport channels for high-performance membranes in vanadium redox flow batteries, ACS Appl. Mater. Interfaces 10 (2018) 32247–32255.

[34] H. Zhang, X. Yan, L. Gao, L. Hu, X. Ruan, W. Zheng, G. He, Novel triple tertiary amine polymer-based hydrogen bond network inducing highly efficient proton-conducting channels of amphoteric membranes for high-performance vanadium redox flow battery, ACS Appl. Mater. Interfaces 11 (2019) 5003–5014.

[35] S. Yun, J. Parrondo, V. Ramani, Derivatized cardo-polyetherketone anion exchange membranes for all-vanadium redox flow batteries, J. Mater. Chem. 2 (2014) 6605–6615.

[36] D. Zhang, X. Yan, G. He, L. Zhang, X. Liu, F. Zhang, M. Hu, Y. Dai, S. Peng, An integrally thin skinned asymmetric architecture design for advanced anion exchange membranes for vanadium flow batteries, J. Mater. Chem. 3 (2015) 16948–16952.

[37] B. Zhang, Q. Wang, S. Guan, Z. Weng, E. Zhang, G. Wang, Z. Zhang, J. Hu, S. Zhang, High performance membranes based on new 2-adamantane containing poly(aryl ether ketone) for vanadium redox flow battery applications, J. Power Sources 399 (2018) 18–25.

[38] Y. Xing, L. Liu, C. Wang, N. Li, Side-chain-type anion exchange membranes for vanadium flow battery: properties and degradation mechanism, J. Mater. Chem. 6 (2018) 22778–22789.

[39] M.S. Cha, S.W. Jo, S.H. Han, S.H. Hong, S. So, T.-H. Kim, S.-G. Oh, Y.T. Hong, J. Y. Lee, Ether-free polymeric anion exchange materials with extremely low vanadium ion permeability and outstanding cell performance for vanadium redox flow battery (VRFB) application, J. Power Sources 413 (2019) 158–166.

[40] X.L. Zhou, T.S. Zhao, L. An, L. Wei, C. Zhang, The use of polybenzimidazole membranes in vanadium redox flow batteries leading to increased coulombic efficiency and cycling performance, Electrochim. Acta 153 (2015) 492–498.

[41] S. Peng, X. Yan, D. Zhang, X. Wu, Y. Luo, G. He, A H_3PO_4 preswelling strategy to enhance the proton conductivity of a H_2SO_4-doped polybenzimidazole membrane for vanadium flow batteries, RSC Adv. 6 (2016) 23479–23488.

[42] L. Hu, L. Gao, X.M. Yan, W.J. Zheng, Y. Dai, C. Hao, X.M. Wu, G.H. He, Proton delivery through a dynamic 3D H-bond network constructed from dense hydroxyls for advanced ion-selective membranes, J. Mater. Chem. 7 (2019) 15137–15144.

[43] X. Yan, J. Sun, L. Gao, W. Zheng, Y. Dai, X. Ruan, G. He, A novel long-side-chain sulfonated poly (2,6-dimethyl-1,4-phenylene oxide) membrane for vanadium redox flow battery, Int. J. Hydrogen Energy 43 (2018) 301–310.

[44] Y. Zhou, L. Yu, J. Wang, L. Liu, F. Liang, J. Xi, Rational use and reuse of Nafion 212 membrane in vanadium flow batteries, RSC Adv. 7 (2017) 19425–19433.

[45] E.-K. Kim, S.Y. Lee, S.Y. Nam, S.J. Yoo, J.Y. Kim, J.H. Jang, D. Henkensmeier, H.-J. Kim, J.-C. Lee, Synthesis of high molecular weight polybenzimidazole using a highly pure monomer under mild conditions, Polym. Int. 66 (2017) 1812–1818.

[46] S. Li, X. Zhu, D. Liu, F. Sun, A highly durable long side-chain polybenzimidazole anion exchange membrane for AEMFC, J. Membr. Sci. 546 (2018) 15–21.

[47] S.S. Peng, X.M. Wu, X.M. Yan, L. Gao, Y.Z. Zhu, D.S. Zhang, J. Li, Q. Wang, G. H. He, Polybenzimidazole membranes with nanophase-separated structure induced by non-ionic hydrophilic side chains for vanadium flow batteries, J. Mater. Chem. 6 (2018) 3895–3905.

[48] B. Schwenzer, J. Zhang, S. Kim, L. Li, J. Liu, Z. Yang, Membrane development for vanadium redox flow batteries, ChemSusChem 4 (2011) 1388–1406.

[49] P. Yang, J. Long, S.S. Xuan, Y.L. Wang, Y.P. Zhang, J.C. Li, H.P. Zhang, Branched sulfonated polyimide membrane with ionic cross-linking for vanadium redox flow battery application, J. Power Sources 438 (2019) 226993–227003.

[50] Y. Ma, L. Li, L. Ma, N.A. Qaisrani, S. Gong, P. Li, F. Zhang, G. He, Cyclodextrin templated nanoporous anion exchange membrane for vanadium flow battery application, J. Membr. Sci. 586 (2019) 98–105.

[51] D.J. Chen, H.N. Qi, T.T. Sun, C. Yan, Y.Y. He, C.Z. Kang, Z.Z. Yuan, X.F. Li, Polybenzimidazole membrane with dual proton transport channels for vanadium flow battery applications, J. Membr. Sci. 586 (2019) 202–210.

[52] K. Geng, Y. Li, Y. Xing, L.H. Wang, N.W. Li, A novel polybenzimidazole membrane containing bulky naphthalene group for vanadium flow battery, J. Membr. Sci. 586 (2019) 231–239.

[53] Y.F. Xia, B. Liu, Y.H. Wang, Effects of covalent bond interactions on properties of polyimide grafting sulfonated polyvinyl alcohol proton exchange membrane for vanadium redox flow battery applications, J. Power Sources 433 (2019) 126680–126688.

[54] Y.X. Zhang, L.Y. Zheng, B. Liu, H.X. Wang, H.F. Shi, Sulfonated polysulfone proton exchange membrane influenced by a varied sulfonation degree for vanadium redox flow battery, J. Membr. Sci. 584 (2019) 173–180.

[55] T. Wang, S.J. Moon, D.S. Hwang, H. Park, J. Lee, S. Kim, Y.M. Lee, S. Kim, Selective ion transport for a vanadium redox flow battery (VRFB) in nano-crack regulated proton exchange membranes, J. Membr. Sci. 583 (2019) 16–22.

[56] L. Ding, X. Song, L. Wang, Z. Zhao, Enhancing proton conductivity of polybenzimidazole membranes by introducing sulfonate for vanadium redox flow batteries applications, J. Membr. Sci. 578 (2019) 126–135.

[57] L.H. Yu, J.Y. Xi, Durable and efficient PTFE sandwiched SPEEK membrane for vanadium flow batteries, ACS Appl. Mater. Interfaces 8 (2016) 23425–23430.

[58] Y. Chen, Z. Liu, M. Lin, Q. Lin, B. Tong, D. Chen, Selectivity enhancement of quaternized poly(arylene ether ketone) membranes by ion segregation for vanadium redox flow batteries, Sci. China Chem. 62 (2019) 479–490.

[59] M.A. Aziz, S. Shanmugam, Sulfonated graphene oxide-decorated block copolymer as a proton-exchange membrane: improving the ion selectivity for all-vanadium redox flow batteries, J. Mater. Chem. 6 (2018) 17740–17750.

[60] J. Ren, Y. Dong, J. Dai, H. Hu, Y. Zhu, X. Teng, A novel chloromethylated/quaternized poly(sulfone)/poly(vinylidene fluoride) anion exchange membrane with ultra-low vanadium permeability for all vanadium redox flow battery, J. Membr. Sci. 544 (2017) 186–194.

[61] B. Zhang, S. Zhang, Z. Weng, G. Wang, E. Zhang, P. Yu, X. Chen, X. Wang, Quaternized adamantane-containing poly(aryl ether ketone) anion exchange membranes for vanadium redox flow battery applications, J. Power Sources 325 (2016) 801–807.

[62] M. Abdiani, E. Abouzari-Lotf, T.M. Ting, P.M. Nia, S.S. Sha'rani, A. Shockravi, A. Ahmad, Novel polyolefin based alkaline polymer electrolyte membrane for vanadium redox flow batteries, J. Power Sources 424 (2019) 245–253.

[63] B. Zhang, E. Zhang, G. Wang, P. Yu, Q. Zhao, F. Yao, Poly(phenyl sulfone) anion exchange membranes with pyridinium groups for vanadium redox flow battery applications, J. Power Sources 282 (2015) 328–334.

[64] L. Hu, L. Gao, X. Yan, "Fishnet-like" ion-selective nanochannels in advanced membranes for flow batteries, J. Mater. Chem. 7 (2019) 21112–21119.